Eur. Phys. J. B **59**, 277–283 (2007)
DOI: 10.1140/epjb/e2007-00292-2

THE EUROPEAN PHYSICAL JOURNAL B

Investigations of "soft-landed" Cd surface atoms via nuclear methods: hyperfine-field sign determination

Y. Manzhur[1], W.-D. Zeitz[1,a], M.J. Prandolini[1], W.D. Brewer[2], P. Imielski[2], J. Schubert[2], K. Johnston[3], and the ISOLDE-Collaboration

[1] Hahn-Meitner-Institut Berlin GmbH, Glienicker Strasse 100, 14109 Berlin, Germany
[2] Freie Universität Berlin, Fachbereich Physik, Arnimallee 14, 14195 Berlin, Germany
[3] CERN, PH DIV, 1211 Genève 23, Switzerland

Received 10 April 2007 / Received in final form 17 July 2007
Published online 26 October 2007 –

Abstract. Using refined preparation techniques, cadmium guest atoms have been positioned at different sites on the surfaces of nickel crystals. The magnetic hyperfine fields and the electric field gradients at the Cd nuclei were measured by time-dependent perturbed angular correlation (TDPAC) spectroscopy of the emitted gamma radiations. By measuring the combined interactions, electric field gradients and magnetic hyperfine fields can be unambiguously attributed to each surface site. The signs of the magnetic hyperfine fields are determined by applying an external magnetic field and choosing the appropriate γ-ray detector configuration. The measured fields correlate with the number of neighbouring host atoms. Band structure calculations confirm this finding and predict magnetic fields for various *sp* elements from the band structure of the *s*-like conduction electrons. The quadrupolar interactions are manifestations of the balance in the occupation of the guest *p*-sublevels. These results provide new information on the structure and formation of electronic configurations of *sp* elements in different local environments and will contribute to understanding electronic effects on surfaces.

PACS. 73.20.-r Electron states at surfaces and interfaces – 75.70.Rf Surface magnetism – 76.80.+y Mossbauer effect; other gamma-ray spectroscopy

1 Introduction

The electronic configurations of atoms on surfaces have frequently been investigated by a variety of methods. The results stood alone until band structure calculations developed to the point of being able to provide a link between the different experiments. Such calculations have been able to obtain the electrostatic potentials and the spin polarizations in the vicinity of the atoms by treating the scattering behavior of valence electrons at the atomic potentials. As these properties are directly correlated to the bonds in the lattice, the large and growing body of results will finally permit a unified model to understand the electronic properties of solid matter.

In the present investigations, we use the nuclear method of time-differential perturbed angular correlation (TDPAC) spectroscopy, which permits the determination of the electric field gradient tensors and the magnetic hyperfine fields at the nuclear sites of guest atoms. The guests may occupy different lattice sites on the surfaces of very clean single crystals and at interfaces between layers consisting of different materials. In a number of experiments using ^{111}In/^{111}Cd probe nuclei on copper [1], silver [2], and palladium [3] surfaces, these sites could be identified by means of the components of the electric field-gradient tensors. A recent calculation for a series of *sp* elements on surfaces, including cadmium [4], was able to correlate the field gradients predominantly to the occupation of the sublevels in the valence *p* band.

The first systematic determinations of the magnetic hyperfine fields for an *sp* element, i.e. cadmium, at different sites on nickel surfaces has recently been published [5,6]. Here again, the electric field gradient serves to identify the specific sites and furthermore, by measuring the combined interactions via TDPAC spectroscopy, a magnetic hyperfine field can be attributed to each site. The most surprising result was the discovery that the 7.3(2) Tesla magnetic field $|\boldsymbol{B}_{hf}|$ at Cd *adatoms* on top of the Ni(100)-surface [6] deviates considerably from $|\boldsymbol{B}_{hf}| = 16.0(8)$ Tesla on the Ni(111)-surface. In their interpretation, the authors propose a correlation between the magnetic hyperfine field and the number of adjacent nickel atoms, i.e. the coordination number NN [6,7]. Similar correlations have been observed in other systems where the hyperfine field of implanted or soft-landed probes was found to depend on the local atomic environment [8–10].

[a] e-mail: zeitz@hmi.de

In the present case of Cd probes on Ni, the correlation of $|\boldsymbol{B}_{hf}|$ with the coordination number is confirmed by two band structure calculations [11,12], which attribute the magnetic hyperfine fields to the polarization of the conduction-electron s band in the vicinity of the impurity nucleus.

However, there is one serious objection to the correlation as given in the earlier publications [5–7]: with the exception of the bulk value [13], the signs of the magnetic fields have not been measured, but rather were postulated in accordance with calculations of selected configurations for Zn atoms on Ni [14]. In order to obtain a smooth curve, the hyperfine fields for Cd on nickel were presumed to change sign between the coordination numbers $NN = 5$ and $NN = 6$. This assumption is contradicted by one of the band structure calculations, based on a Green's function method, which predicts an abrupt crossover from negative hyperfine fields to large positive values between the coordination numbers $NN = 4$ and $NN = 5$ [11]. In a second model using a supercell approach [12], and taking lattice relaxation into account, a quadratic correlation to the coordination number was reproduced, as proposed in the interpretation of the experiments.

By applying a sign-sensitive technique in the current investigations, we were able to carry out measurements to resolve this controversy. The result will be relevant to the question as to what extent band structure calculations can be relied upon for predictions of the electronic configurations at surfaces. The electronic configurations play a role in bonding, catalysis at local sites, magnetic interactions and spin dynamics, for example, and in the structures of objects of limited dimensions. The results of the experiments and the calculations will give insight into the basic mechanisms involved.

2 Experimental

The application of TDPAC spectroscopy requires the delivery of appropriate radioactive isotopes. For these experiments, which were performed at the on-line mass separator ISOLDE at CERN in Geneva, ^{111}In and $^{111\mathrm{m}}$Cd radioactive isotopes were produced through reactions with high-energy protons, ionized on hot metal surfaces or by laser excitation, and extracted from the ion source by applying a 60 kV potential. After mass separation, the ions are collected in a molybdenum catcher foil which is mounted in the prechamber of the experimental apparatus.

Before the deposition of the radioactive atoms, the crystal surfaces are cleaned and reconstructed in the main UHV chamber in successive preparation cycles of alternating argon sputtering and annealing. After each cycle, the surface quality is analyzed by Auger and LEED spectroscopy. In order to maintain the crystal surface clean and undamaged, a special preparation technique is used for soft landing of the radioactive elements. Further details of the preparation method can be found in [15].

It has been found that metals such as In or Cd may easily be manipulated to occupy specific sites on metal surfaces by annealing procedures. At temperatures below 35 K for Ni(111) and 77 K for Ni(100), most atoms are found on terrace sites, which they occupy directly after soft landing. At temperatures between 120 K and 250 K, the atoms move to free step sites or kinks at the edges of incomplete layers. At higher temperatures, they are incorporated mainly in substitutional step sites or substitutional terrace sites in the surface layer (above 470 K for Ni(100)). The specific sites can be identified by the quadrupolar interactions, since the electronic charge distribution at the surface will not be cubic in most cases. Examples of this technique have been given for the surfaces of non-magnetic metals [1–3], but the experiments for Cd on nickel represent the first comprehensive systematics for the surface of a ferromagnetic material.

The guest configurations are produced with the ^{111}In ($T_{1/2} = 2.83$ d) or the $^{111\mathrm{m}}$Cd ($T_{1/2} = 49$ min) precursor nuclei, which have sufficiently long lifetimes to allow the preparation procedures to be carried out. As the recoil in the decay to the TDPAC nucleus is sufficiently low, the lattice site is undisturbed and this permits the observation of the hyperfine interactions in the ^{111}Cd isomeric $I = 5/2$ level ($T_{1/2} = 85$ ns) using TDPAC spectroscopy. This isomeric level is populated and depopulated through a γ-γ cascade accompanied by emission of γ-rays of specific energies. After the extraction of the lifetime from the time spectrum by computing the ratio function $R(t)$, time-dependent oscillation spectra are obtained. For the isomeric level, with a nuclear spin $I = 5/2$, one spectrum with a combined interaction contains up to 15 frequencies which are determined by a set of eight parameters. Examples of a measured and analyzed spectrum are shown in Figure 1.

For quadrupolar interactions with cylindrical electric field gradients (EFG), the TDPAC oscillations are determined by the smallest observable interaction frequency ω_0:

$$\omega_0 = 6e_oQV_{zz}/\hbar(4I(2I-1)) \tag{1}$$

(for half-integral spins). In this formula, $I = 5/2$ is the nuclear spin of the isomeric ^{111}Cd level and $Q = +0.83(12)$ b [16] is the nuclear quadrupole moment. The quantity V_{zz} stands for the largest diagonal tensor component of the traceless symmetric EFG tensor. The second of the five tensor elements, the asymmetry parameter $\eta = (V_{xx} - V_{yy})/V_{zz}$ $(0 \leqslant \eta \leqslant 1)$, describes the deviation from cylindrical symmetry. Three Euler angles describe the orientation of the diagonal tensor with respect to the fixed coordination system which is defined by the crystal axes or the detector positions.

A purely magnetic interaction of the nuclear magnetic moment with the hyperfine field $|\mathbf{B}_{hf}|$ yields the Larmor frequency ω_L,

$$\omega_L = -g\mu_{_N} B_{hf}(T)/\hbar. \tag{2}$$

The nuclear g-factor $g = -0.3062(10)$ of the isomeric 5/2 level is known [17]. $B_{hf}(T)$, the strength of the magnetic field, and two angles which characterise the alignment of $|\mathbf{B}_{hf}|$ are three further parameters, thus giving eight in

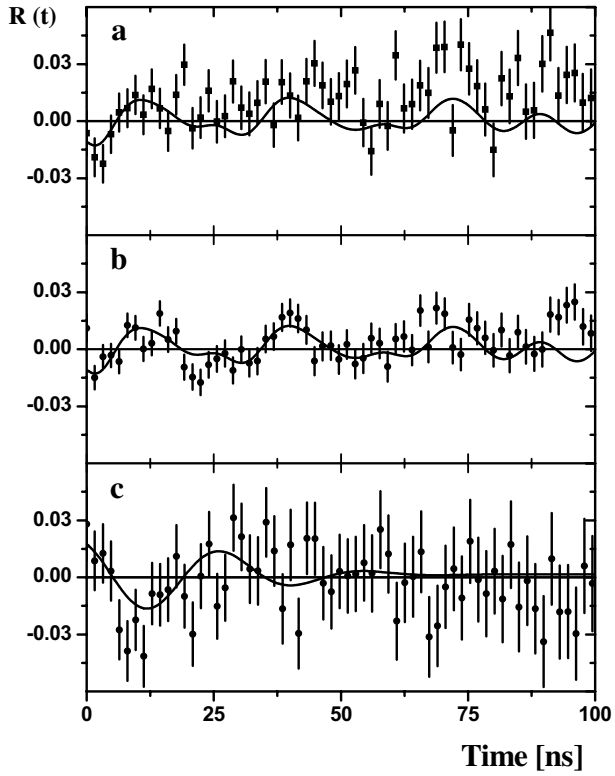

Fig. 1. The measured PAC spectra of ^{111}In/^{111}Cd on the Ni surfaces in the 135°/−135° detector configuration. The signs of the magnetic hyperfine fields for the coordination numbers $NN = 5$, $NN = 6$ (top: a), for $NN = 6$ and $NN = 7$ (middle: b) and for $NN = 4$ (bottom: c) can be directly determined from the onset of the oscillation. An external magnetic field was applied.

all. In the case of a combined interaction, the angle between V_{zz} and B is used as one of the parameters. In total, $n = I(2I+1)$ interaction frequencies and their amplitudes have to be calculated for each special experimental arrangement. The frequencies and their amplitudes characterise the site of the atom on the surface and the measured magnetic field at that site.

The ratio function $R(t)$ shown in Figure 1,

$$R(t) = [I(135°) - I(-135°)]/[I(135°) + I(-135°)] = (3A_{22}\sin 2\omega t)/(4 + A_{22}) \approx \sin 2\omega t. \quad (3)$$

is calculated from the time-dependent perturbed angular correlation coincidence spectra $I(135°)$ and $I(-135°)$ of the detectors and displays sinusoidal oscillations which are sensitive to the phase of the initial Larmor precession (in contrast to the usually-observed cosine oscillations, which are insensitive to this initial phase). In the detector geometry chosen, coincidence spectra are recorded for pairs of detectors positioned at 135° and at −135° relative to one another. Details of the technique are given elsewhere [18].

The sign of the magnetic hyperfine field is defined with respect to an externally applied magnetic field. Two gold-plated permanent magnets were installed in the UHV chamber; they deliver a sufficiently large magnetic field of

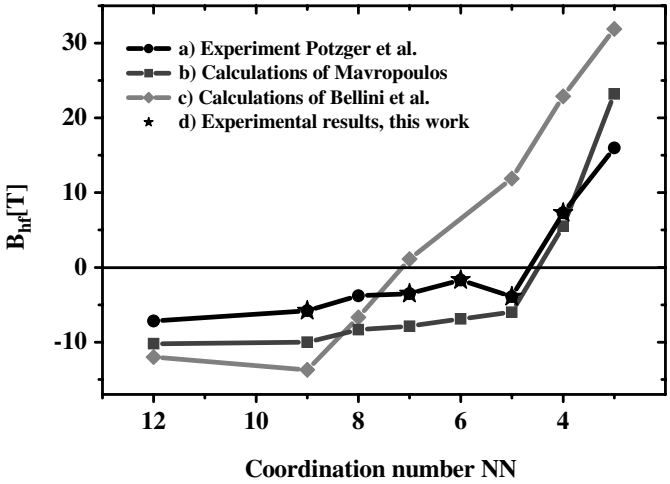

Fig. 2. Coordination number dependence of B_{hf} of Cd on Ni. The symbols refer to different measurements and calculations: (a) experimental results taken from Potzger et al. [5,6] for surface sites and from Shirley et al. [13] for the substitutional lattice site ($NN = 12$); (b) band structure calculations using the real-space Green's function embedding method [11]; (c) band structure calculations using the supercell method [12]; (d) magnitudes and signs of magnetic hyperfine fields as determined in this work.

$B_{ext} = 0.05$ T to align the ferromagnetic domains in the nickel samples.

In Figure 1, the measured perturbed angular correlation spectra which are relevant for the determination of the signs of the magnetic fields for various coordination numbers are shown. As can be seen directly from the initial phases of the oscillations in each spectrum, the configurations with $NN = 7$, $NN = 6$ and $NN = 5$ have negative hyperfine fields. The same is true for $NN = 9$, whose spectrum is not shown here. In contrast, the site with $NN = 4$ on the ⟨100⟩ surface of nickel exhibits a positive field. The values of the parameters which are found in the analysis of these spectra agree with those found with the 90° standard detector arrangement which was used in previous investigations.

A compilation of all the observed magnetic hyperfine fields for Cd on Ni is shown in Figure 2, correlated to the respective coordination numbers. The magnitude and sign of the magnetic field at Cd in fcc Ni on a regular lattice site, $B_{hf}(T = 4.2\text{ K}) = -7.1(5)$ T, have been known for some time [13]. The magnetic field which is given here takes into account the recalibrated nuclear g-factor. The signs of the other fields, which are indicated by stars in Figure 2, were determined in the current investigation. Especially the allocation of the sign for $NN = 5$ is in contradiction to that of the earlier interpretation. There is a sudden change of hyperfine field sign between $NN = 5$ and $NN = 4$, which gives a clear preference for the results of the band structure calculation using the real space Green's function embedding method [11]. For $NN = 3$, the sign has not been measured, but the systematics curve leaves little doubt that it is positive.

3 Interpretation

The interpretation of the magnetic hyperfine fields and the electric field gradients at isolated Cd impurities on the surface and in the bulk of nickel is based on the local level densities of the itinerant fraction of the s and p electrons at the impurity site. Density-functional calculations for series of sp elements in ferromagnetic hosts have shown that the quadrupolar interaction is predominantly determined by the balance of occupation of the sublevels of the highest p states, whereas the magnetic interactions can be attributed to the polarization of the electrons in the s-like conduction band.

We first discuss the field gradients. In order to determine the components of the field gradient tensor $V_{\alpha\beta}(\boldsymbol{r}_0)$, the electrostatic potential $\varphi(\boldsymbol{r}_0)$ which is present at the nuclear site $\boldsymbol{r}_0$ of the impurity has to be calculated:

$$\varphi(\boldsymbol{r}_0) = \int \rho(\boldsymbol{r})/(\boldsymbol{r} - \boldsymbol{r}_0) d^3r. \quad (4)$$

In the integral, the nuclear charges are included as the Coulomb potential of the positive point charges at the lattice sites, and negative charge densities to $\rho(\boldsymbol{r})$ are derived from the electronic wave functions of electrons in the neighbourhood of the impurity. Bond lengths as well as the distances $(\boldsymbol{r} - \boldsymbol{r}_0)$ are allowed to change when lattice forces are relaxed.

Taking the second derivatives yields the components $V_{\alpha\beta}(\boldsymbol{r}_0)$ of the field gradient tensor:

$$V_{\alpha\beta}(\boldsymbol{r}_0) = (\partial^2\varphi(\boldsymbol{r}_0)/(\partial\alpha\ \partial\beta) - (1/3)\,\delta_{\alpha\beta}\nabla^2\varphi\,(\boldsymbol{r}_0). \quad (5)$$

Here α, β stand for the respective pair of Cartesian coordinates and the Laplace operator in the second part of the equation has been introduced to give a traceless tensor. The largest diagonal component is chosen to be V_{zz}, and the asymmetry parameter is defined by $\eta = (V_{xx} - V_{yy})/V_{zz}$.

As cubic arrangements of charges around $\boldsymbol{r}_0$ give vanishing gradients, s electrons do not contribute to the field gradient at the nucleus. In sp-element impurities, the p electrons are dominant and the contribution from d electrons is small. Guided by the idea that oblate electronic charge distributions give positive field gradients and prolate distributions produce negative gradients, the measured field gradient of cylindrical charge distributions may be deduced from the occupation of the highest p_x and p_y levels in relation to the occupation of the p_z-level:

$$V_{zz} \sim \Delta n_p = \frac{1}{2}\,(n_{px} + n_{py}) - n_{pz}. \quad (6)$$

The occupation numbers n_{pi} are found by integrating over the densities of the highest occupied p sublevels. Results of the calculations for Cd on Pd [4] are shown in Figure 3 together with the experimental field gradients for Cd on Ni surfaces ([6,7], this work).

The observed cylindrically-symmetric field gradients at Cd on metal surfaces can easily be understood from the above principles: for guest sites in the surface layers, the predominant occupation of the $p_x + p_y$ levels gives strong positive field gradients. The signs cannot be measured by TDPAC spectroscopy but may be taken from model calculations. At adatoms which are on top of the surface, the p_z level is filled to a comparable degree, and a small positive field gradient is found for Cd on Ni(100), and even a negative one on Ni(111). The dominance of the p_x and the p_y levels persists in non-cylindrical configurations of Cd as long as the sites are not on top of the layer. In order to find some characterization for the configurations, we propose counting the Ni atoms which are adjacent to Cd in the top layer (NN_1) and the layer below the Cd impurity (NN_2) separately. These numbers are given as pairs (NN_1, NN_2) in Figure 3.

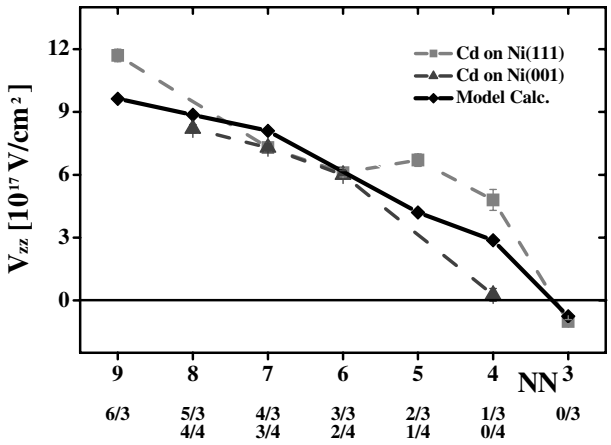

Fig. 3. Electric field gradients at Cd impurities on Ni surfaces. The absolute values of the gradients are taken from previous experiments [7,31] and from this work. The results are compared to model calculations for Cd on Pd (solid line) [4]. The gradients are assumed to depend roughly on the coordination numbers NN. The pairs of numbers which are given below the figure refer to the numbers of neighbouring host atoms in the top layer, NN_1, and the layer below the top layer, NN_2, on the $\langle 111\rangle$ and the $\langle 100\rangle$ surfaces of Ni.

Secondly, we discuss the magnetic hyperfine fields of isolated sp elements on the surfaces of ferromagnets. Here, we propose a correlation between the fields at impurities in surface sites with the field they would experience on substitutional sites in the bulk. Bulk values show regularities across each sp element period in the periodic table of elements [19,20]. This regularity can be ascribed entirely to the Fermi contact interaction of polarised s electrons in the conduction band [21,22]. As the d shells are empty or completely filled for the sp elements and local electronic moments are expected to be negligible, neither core polarisation nor orbital motions will give significant contributions. As long as the d shells are closed, transition elements like Zn and Cd can also be included in this category.

Especially when lattice relaxation is taken into account, ab initio calculations yield the experimentally determined fields for impurities in Fe [23,24]. For unknown reasons, the agreement between measured and calculated values is still poor for impurities in Ni [25]. In all systems

investigated, the systematic trends in the magnetic fields across the periods of *sp* elements are similar and can be attributed to peak structures which develop in the level densities of scattered *s* electrons. Local level densities with similar shapes were also found for guest atoms on nickel surfaces [11,14].

In order to obtain predictions for the magnetic fields, details of the level densities in the local *s*-like conduction band at the guest atoms have to be known. In the vicinity of the Fermi level, two structures can be distinguished, separated by a clearly visible dip which is even visible for *sp*-elements in the bulk [21,22]. At energies in the range of −8 eV to −4 eV below the Fermi level, "bonding states" are found. They are fully occupied in all *sp*-element atoms in metals. The negative hyperfine fields they produce originate from a spin-dependent *s*-*d* exchange interaction with the *d* orbitals of the magnetic host atoms. On the other hand, positive contributions to the magnetic field $\boldsymbol{B}_{hf}$ are obtained from an excess of majority electrons in the "anti-bonding region" above the dip which is located immediately below and above the Fermi level. The maxima of spin-up and spin-down level densities are located at different energies. As a consequence, the total hyperfine field $\boldsymbol{B}_{hf}$ is a superposition of the two components:

$$\boldsymbol{B}_{hf}(\text{total}) = \boldsymbol{B}_{hf}(\text{bonding}) + \boldsymbol{B}_{hf}\left(\int_{E_{dip}}^{E_F} |\rho_s^{\uparrow} - \rho_s^{\downarrow}| dE\right). \tag{7}$$

The energies E_{dip} and E_F characterize the positions of the dip and the Fermi level, respectively. The filling of the "anti-bonding" levels is different for each impurity element, as it depends on the position of the Fermi level. The strength of the field results sensitively from the balance of populations between the majority band $\rho_s^{\uparrow}$ and the minority band $\rho_s^{\downarrow}$. Further details of the calculations may be taken from preceding papers [20–25].

The comprehensive study of magnetic fields at Cd in surface sites which is available from this work allows a test of these concepts. When the impurities are implanted onto surfaces, the number of neighbours will be reduced and the peak structures will change. In substitutional lattice sites in fcc-nickel ($NN = 12$), the negative hyperfine field at Cd is produced by the bonding levels, as most of the anti-bonding peak structure is located at energies above the Fermi level. In surface sites, the peak structures are pulled in the direction of the Fermi level and, in consequence, the overall negative fields become weaker. Positive magnetic fields are predicted when the peak in the majority band of the anti-bonding structure crosses the Fermi level, just before $NN = 4$. Even for $NN = 3$, the occupied levels in the majority band below E_F give rise to large positive fields.

The above view is supported by the results of two ab initio band structure calculations [11,12]. Both models can reproduce the correlation between the magnetic fields of Cd on nickel surfaces and the coordination numbers, and they correctly predict the positive signs for adatoms. Our ability in the present investigation to determine the signs of the magnetic hyperfine fields shows that there is an abrupt change in the fields between $NN = 5$ and $NN = 4$. This finding contradicts the calculated magnetic fields which are found using the supercell method [12] and which are shown in the plots. The real-space Green's function embedding method [11], on the other hand, is correct in its predictions of the signs of the magnetic fields for all Cd sites observed.

Further support for this concept can be found in the hyperfine fields at Se on nickel. Se has a strong positive magnetic field when implanted into substitutional sites in the bulk. For adatom configurations, the excess of spin-up electrons is compensated by filling spin-down levels, while all the anti-bonding levels move below the Fermi level. As a consequence, a very small field is predicted for Se on Fe and Ni [14]. This prediction was already verified by the observations of Se on Fe, Co, and Ni surfaces [26,27].

4 Conclusions

The following rules of thumb may be drawn from the above observations: the positions of the anti-bonding levels with respect to the Fermi level correlate with the shielded Coulomb potential of the impurity nucleus [21]. The widths of the anti-bonding bands are gradually reduced with decreasing numbers of neighbours, and the anti-bonding levels are pulled below the Fermi level [11,14]. The ultimate limit of this process will be reached when the guest becomes a free atom.

These rules are based on calculations using density-functional theory. With a growing number of experimental results being interpreted with the help of these theories, the magnetic hyperfine fields and the electric field gradients can be linked to parameters which are commonly used in complementary techniques in solid state physics. In the nuclear techniques, the information is obtained from the hyperfine interaction between the nuclear moments and the charge distributions, and the magnetic moments of the electrons. The interaction is expected to persist when atoms are embedded into crystal lattices where the probe nuclei serve as spectators, detecting changes in the electronic wave functions with respect to free atoms. For the non-magnetic *sp*- elements, the changes in the structures of *s* electron and *p* electron densities can be considered separately: the *s* electrons are responsible for the magnetic part of the interaction, while the quadrupolar interaction can be attributed to the occupation of the *p* levels. As the outer *p* shells are empty in free Cd atoms, the predicted occupations of *p* levels may be taken as evidence for the existence of partial waves after electron scattering on the impurity potential, as were predicted by the Friedel model [28].

In order to estimate the magnetic hyperfine fields, the real-space Green's function embedding method [11,14] uses the wave functions of the undisturbed nickel lattice and, in an iterative process, computes the changes which are introduced by scattering the electrons on the impurity potential. This method, even though lattice relaxation was

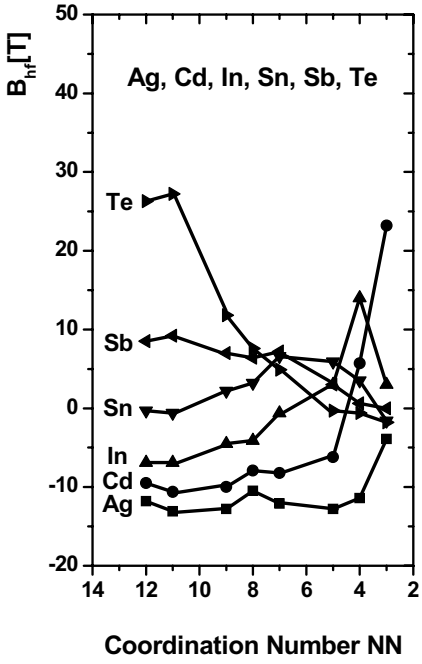

Fig. 4. Predicted magnetic hyperfine fields for some 5*sp* elements in different sites on the rigid nickel surface (reproduced from [11]). Lattice relaxations are not included. The expected fields correlated with the coordination numbers NN and depend on the spin-resolved level densities in the conduction band of scattered s electrons.

not included, is thus more appropriate for use in calculating magnetic hyperfine fields at guest atoms on clean bulk surfaces than the supercell method of reference [12].

As long as the electronic charge distributions exhibit long-range oscillations, the inclusion of lattice relaxation may not be regarded as essential. Especially for the s electrons, recent STM measurements show that charge oscillations which are produced by scattered electrons can have wavelengths up to 15 Å [29,30]. On the other hand, calculations will run into inconsistencies when lattices are built up of clusters which are smaller than the wavelength of the oscillations. This remark applies to the supercell method [12], because in this method the lattice is simulated by repetition of identical atomic arrangements, called "slades". The results of the procedure lack coherence if the sizes of the local clusters cannot be increased until the predicted quantities are insensitive to changes in lateral dimensions and thicknesses of the slades. The magnetic fields listed in reference [12] indicate that the calculations were not able to meet this criterion.

Finally, in Figure 4, the predicted magnetic fields for some *sp* elements in the fifth period of the periodic table are shown. The values were taken from the Green's function work [11]. These predictions can be regarded with confidence since the agreement with the measured hyperfine fields at Cd on different sites on the Ni surface has proved to be satisfactory. For elements of the fourth period, similar calculations have been carried out for selected configurations [14]. In all these cases, the magnetic fields reflect the polarisation of s-like conduction electrons on an atomic scale. The structures of level densities below and above the Fermi levels are similar for all *sp* elements, and the differences among elements are mainly attributable to the energetic location of the Fermi level. In accordance with the bulk values, the behavior of the magnetic fields going across the periods nicely correlates with the energies of the highest occupied s levels in the free atoms [21,22]. From these features, the properties of *sp* elements in different environments are predictable, which is not, at first sight, obvious from their observed behavior.

We thank the staff of CERN-ISOLDE and of the Hahn-Meitner-Institut for assistance with apparatus and measurements. One of us (MJP) thanks for Deutsche Forschungsgemeinschaft (DFG) for support during this work. We are especially grateful to the late H.H. Bertschat for his dedication to this project.

References

1. T. Klas, R. Fink, G. Krausch, R. Platzer, J. Voigt, R. Wesche, G. Schatz, Europhys. Lett. **7**, 151 (1988)
2. R. Wesche, R. Fink, T. Klas, G. Krausch, R. Platzer, J. Voigt, G. Schatz, J. Phys.: Condens. Matter **1**, 7407 (1989)
3. E. Hunger, H. Haas, Surf. Sci. **234**, 273 (1990)
4. S. Cottenier, V. Bellini, M. Cakmak, F. Manghi, M. Rots, Phys. Rev. B **70**, 155418 (2004)
5. K. Potzger, A. Weber, H.H. Bertschat, W.-D. Zeitz, M. Dietrich, Phys. Rev. Lett. **88**, 247201 (2002)
6. K. Potzger, A. Weber, W.-D. Zeitz, H.H. Bertschat, M. Dietrich, Phys. Rev. B **72**, 054435/1 (2005)
7. M.J. Prandolini, Y. Manzhur, A. Weber, K. Potzger, H.H. Bertschat, H. Ueno, H. Migoshi, M. Dietrich, Appl. Phys. Lett. **85**, 76 (2004)
8. M. Neubauer, K.P. Lieb, P. Schaaf, M. Uhrmacher, Phys. Rev. B **53**, 10237 (1996)
9. U. Kohl, C. Cecco, M. Dippel, G. Filleböck, B.-U. Runge, G. Schatz, Hyp. Int. **120–121**, 303 (1999)
10. R. Kirsch, M.J. Prandolini, O. Beutler, W.D. Brewer, M. Gruyters, J. Kapoor, D. Riegel, H. Ebert, S. Frota-Pessôa, Europhys. Lett. **59**, 430 (2002)
11. Ph. Mavropoulos, J. Phys.: Condens. Matter **15**, 8115 (2003)
12. V. Bellini, S. Cottenier, M. Cakmak, F. Manghi, M. Rots, Phys. Rev. B **70**, 155419 (2004)
13. D.A. Shirley, S.S. Rosenblum, E. Matthias, Phys. Rev. **170**, 363 (1968)
14. Ph. Mavropoulos, N. Stefanou, B. Nonas, R. Zeller, P.H. Dederichs, Phys. Rev. Lett. **81**, 1505 (1998)
15. K. Potzger, H.H. Bertschat, A. Burchard, D. Forkel-Wirth, H. Granzer, H. Niehus, S. Seeger, W.-D. Zeitz, ISOLDE Collaboration, Nucl. Instr. Meth. Phys. Res. B **146**, 618 (1998)
16. P. Herzog, K. Freitag, M. Reuschenbach, H. Walitzki, Z. Phys. A **294**, 13 (1980)
17. R.B. Firestone, V.S. Shirley, *Table of Isotopes*, 8th edn. (John Wiley and Sons, New York, 1996)

18. V. Samohvalov, Ph.D. thesis, Technische Universität Bergakademie Freiberg/Germany, Freiberg, 2003
19. G.N. Rao, Hyp. Int. **24**–**26**, 1119 (1985)
20. H. Akai, M. Akai, S. Blügel, R. Zeller, P.H. Dederichs, J. Magn. Magn. Mater. **45**, 291 (1984)
21. H. Katayama-Yoshida, K. Terakura , J. Kanamori, J. Phys. Soc. Jap. **48**, 1504 (80)
22. J. Kanamori, H.K. Yoshida, K. Terakura, Hyp. Int. **9**, 363 (1981)
23. T. Korhonen, A. Settels, N. Papanikolaou, R. Zeller, P.H. Dederichs, Phys. Rev. B **62**, 452 (2000)
24. S. Cottenier, H. Haas, Phys. Rev. B **62**, 461 (2000)
25. H. Haas, Hyp. Int. **151/152**, 173 (2003)
26. H. Granzer, H.H. Bertschat, H. Haas, W.-D. Zeitz, J. Lohmüller, G. Schatz, Phys. Rev. Lett. **77**, 2461 (1996)
27. A. Weber, Ph.D. thesis, Freie Universität Berlin/Germany, Berlin, 2001
28. E. Daniel, J. Friedel, J. Phys. Chem. Solids **24**, 1601 (1963)
29. F. Moresco, L. Gross, M. Alemani, K.-H. Rieder, H. Tang, A. Gourdon, C. Joachim, Phys. Rev. Lett. **91**, 036601 (2003)
30. L. Gross, F. Moresco, L. Savio, A. Gourdon, C. Joachim, K.-H. Rieder, Phys. Rev. Lett. **93**, 056103 (2004)
31. K. Potzger, Ph.D. thesis, Freie Universität Berlin/Germany, Berlin, 2001